Nat Chem. Author manuscript; available in PMC 2020 March 16.

Published in final edited form as:
Nat Chem. 2019 November 01; 11(11): 1049–1057. doi:10.1038/s41557-019-0324-8.

Enzymatic control of cycloadduct conformation ensures reversible 1,3 dipolar cycloaddition in a prFMN dependent decarboxylase

Samuel S. Bailey[1], **Karl A. P. Payne**[1], **Annica Saaret**[1], **Stephen A. Marshall**[1], **Irina Gostimskaya**[1], **Iaroslav Kosov**[1], **Karl Fisher**[1], **Sam Hay**[1,*], **David Leys**[1,*]

[1]Manchester Institute of Biotechnology, School of Chemistry, University of Manchester, 131 Princess Street, M1 7DN Manchester, UK

Abstract

The UbiD enzyme plays an important role in bacterial ubiquinone (coenzyme Q) biosynthesis. It belongs to a family of reversible decarboxylases that interconvert propenoic or aromatic acids with the corresponding alkenes or aromatic compounds using a prenylated flavin (prFMN) cofactor. This cofactor is suggested to support (de)carboxylation through a reversible 1,3-dipolar cycloaddition process. Here we report an atomic-level description of the reaction of the UbiD related ferulic acid decarboxylase with substituted propenoic and propiolic acids (data ranging from 1.01 to 1.39 Å). The enzyme is only able to couple (de)carboxylation of cinnamic acid-type compounds to reversible 1,3-dipolar cycloaddition, while formation of dead-end prFMN cycloadducts occurs with distinct propenoic and propiolic acids. The active site imposes considerable strain on covalent intermediates formed with cinnamic and phenylpropiolic acids. Strain reduction through mutagenesis negatively affects catalytic rates with cinnamic acid, indicating a direct link between enzyme-induced strain and catalysis that is supported by computational studies.

Many enzymes make use of covalent catalysis to achieve substantial rate enhancements, often by recruiting cofactors such as PLP[1], TPP[2] and flavins[3]. To ensure high turnover, these enzymes are inherently required to ensure both rapid and reversible cofactor-ligand adduct formation. In the case of the UbiD enzyme family, reversible decarboxylation has been suggested to occur via a 1,3-dipolar cycloaddition process between the substrate and the UbiD-cofactor, prenylated FMN (prFMN)[4], enabled by the azomethine ylide character of the

*corresponding authors: sam.hay@manchester.ac.uk; david.leys@manchester.ac.uk.

Author contributions

SSB cloned, expressed and purified *An*Fdc1 and various variants. SSB determined all crystal structures with guidance from DL. KAPP generated various *An*Fdc1 variants, and collected solution data with cinnamic acid. AS assisted with crystallisation of the **Int3^{crotonic}** state. SAM assisted with *An*Fdc1 reconstitution. IG assisted with crystallisation of FMN substitued AnFdc1 and the **Int3^{butynoic}** state (with help from IK). KF assisted with protein purification and solution data collection and analysis. SH performed all computational studies. All authors discussed the results and participated in writing of the manuscript. DL initiated and directed this research.

Competing interests

The authors declare no competing interests.

Europe PMC Funders Author Manuscripts

latter. While 1,3-dipolar cycloaddition is commonly used in organic synthesis[5], here we describe this particular process in enzymatic catalysis. Diels-Alder reactions have also recently been found to be catalysed by dedicated enzymes[6], but these are not reported to be reversible. Similarly, 1,3-dipolar cycloaddition reactions such as biocompatible 'click'-chemistry are not considered reversible[7], although the possibility of force-induced cycloreversion is a recent and controversial topic[8–11]. In the case of the fungal ferulic acid decarboxylase **(**Fdc) UbiD-enzyme[12], 1,3-dipolar cycloaddition between prFMN^{iminium} and the cinnamic acid substrate (Fig 1) is proposed to lead to an initial pyrrolidine cycloadduct (**Int1**) that supports decarboxylation concomitant with ring opening, resulting in formation of a distinct prFMN-alkene adduct (**Int2**). A conserved Glu residue is proposed to donate a proton to the alkene moiety, leading to a second pyrrolidine cycloadduct (**Int3**). Finally, the reaction cycle concludes with cycloelimination of **Int3**, leading to alkene product formation and release. The reaction is readily reversible at elevated [CO_2] [12]. There is no direct experimental evidence that any of the proposed intermediates exist, although indirect evidence supporting this mechanism has been reported[13]. Alternative mechanisms proposed to occur with distinct forms of the cofactor have been discounted[14]. However, it remains unclear how the enzyme is able to ensure reversibility of the 1,3-dipolar cycloaddition steps. We aimed to determine whether detailed structural insights could be gained into catalysis by *A. niger* Fdc1, an enzyme used as a model prFMN decarboxylase by virtue of the fact it yields atomic resolution crystal structures[12].

Results

Structure of the *An*Fdc1 substrate complex

Catalytically competent *An*Fdc1 crystals were made by avoiding illumination of the protein during sample preparation and crystallisation, preventing photo-induced cofactor isomerisation and inactivation[14]. Incubation of crystals with cinnamic acid for brief periods of time (typically 10-15 seconds) led to rapid sample deterioration, likely due to styrene accumulation. Electron density obtained with diffraction data from cinnamic acid soaked crystals (prior to crystal dissolution) unambiguously revealed the location of the substrate benzyl moiety above the prFMN^{iminium} isoalloxazine ring system, but revealed density corresponding to multiple conformations of the substrate acrylic acid moiety (*vide infra*). In contrast, rapid soaking and flash-cooling of crystals with alpha-fluorocinnamic acid revealed clear density for the substrate positioned directly above the prFMN^{iminium} azomethine ylide functionality (*i.e.* **Sub** complex, to 1.1 Å resolution; Fig 2a). We could confirm that cinnamic acid binds to the protein in the same conformation, by using inactive *An*Fdc1 crystals that contained FMN rather than prFMN^{iminium} (to 1.26 Å resolution; Supplementary Fig 1a). In the case of the alpha-fluorocinnamic acid prFMN complex, the substrate Cα and Cβ carbons are located directly above the prFMN^{iminium} C1' and C4a (Fig 1), at distances of 3.0 Å and 3.4 Å respectively, in a reactive conformation compatible with the proposed cycloaddition.

The E282Q *An*Fdc1 variant allows structure determination of the Int2 covalent adduct

In order to determine whether covalent adducts (either **Int1** or **Int2**) might accumulate in the absence of the Glu282 mediated protonation step, we sought to determine the crystal

structure of the inactive *An*Fdc1 E282Q variant[14] in complex with cinnamic acid and cinnamic acid derivatives. Indeed, UV-Vis spectroscopy of *An*Fdc1 E282Q incubated with cinnamic acid leads to formation of a distinct spectral species, indicative of adduct formation (Supplementary Fig 2a). The E282Q crystal structure obtained by co-crystallisation with cinnamic acid reveals a covalent prFMN-substrate complex, corresponding to the proposed **Int2** species following decarboxylation (to 1.18 Å resolution; Fig 2b). The substrate alkene bond retains the *trans* configuration but substantially deviates from ideal planar geometry, with a torsional angle of τ = ~112° (as opposed to 180° for a planar *trans* configuration) and an elongated Cα=Cβ bond length of 1.37 Å. Exchange of the bound cinnamic acid for alpha-fluorocinnamic acid or pentafluorocinnamic acid readily occurs *in crystallo*, demonstrating a **Sub** ⇌ **Int2 + CO_2** equilibrium exists in E282Q (Supplementary Fig 1b,c). The alpha-fluorocinnamic acid **Int2** structure (to 1.13 Å resolution) directly demonstrates *syn*-pyramidalisation[15] of the substrate alkene Cα (pyramidalisation angle of ϕ ~20°), which is likely to be a result of the torsional strain imposed. The observed alkene distortion is a likely consequence of the firm hold the enzyme active site exerts on the substrate phenyl moiety, held in place by I187, I327 and F437 at a position directly above and stacked with the prFMN plane. For all E282Q **Int2** structures, the prFMN C1' is located further out of the prFMN plane by ~0.4 Å when compared to other prFMN single bond adduct species (*i.e.* PDB 4ZA9; Fig 2c). In the case of cinnamic acid E282Q **Int2**, this places the Cβ directly above the prFMN C4a at a distance of 3.04 Å, while the Cα atom is in close proximity (~3.2 Å) of the location occupied by the Glu282 carboxylate moiety in the wild-type enzyme structure.

Structure of cycloadducts Int1' and Int3' formed with alkyne compounds

The substrate and product alkyne analogues phenylpropiolic acid and phenylacetylene were used to determine whether cycloadducts **Int1** and/or **Int3**, respectively can be observed in the wild-type enzyme. These compounds can also act as dipolarophiles, but cycloaddition will lead to the double bond-containing 3-pyrroline **Int 1'** rather than the pyrrolidine cycloadducts (Fig 1). Upon addition of either alkyne compound, a clear shift is observed in the enzyme UV-Vis spectrum indicating modification of the $prFMN^{iminium}$ cofactor, with the formation of a species distinct from the E282Q **Int2** adduct (Supplementary Fig 2b). Stopped-flow experiments reveal the formation of this alkyne intermediate occurs with k_{obs} = 101.5 ± 0.4 s^{-1} (Supplementary Fig 3), but following prolonged incubation no product formation could be observed (Supplementary Fig 2c). To investigate the phenylpropiolic acid complex prior to reaction (i.e. **Inhib** complex), inactive crystals of *An*Fdc1 (with prFMN in a semiquinone radical form) were used, revealing the inhibitor (to 1.29 Å resolution) binds in a similar manner to the alpha-fluorocinnamic acid:prFMN or cinnamic acid substrate:FMN complexes obtained. This positions the alkyne Cα and Cβ directly above the $prFMN^{radical}$ C1' and C4a at distances of 3.3 Å and 3.7 Å (Supplementary Fig 1d). In contrast, crystals of active *An*Fdc1 co-crystallised with phenylpropiolic acid (to 1.01 Å resolution) or soaked with phenylacetylene (to 1.10 Å resolution) revealed clear density for a 3-pyrroline cycloadduct (**Int3'**, analogous to the proposed **Int3**) formed between the alkyne moiety and the $prFMN^{iminium}$ (Fig 3a). Hence, surprisingly, the phenylpropiolic acid derived adduct lacked density for the carboxylate moiety, and was highly similar to that obtained with phenylacetylene (Supplementary Fig 1e). This suggests decarboxylation has

occurred over the prolonged time frame required for co-crystallisation (typically exceeding 24 hours). Indeed, when using a rapid soaking procedure as an alternative approach, a distinct cycloadduct (**Int1'**; to 1.21 Å resolution) is observed that retains the carboxyl moiety attached to the prFMN C1' group (and thus resembles the proposed **Int1**; Fig 3b). We used a mass spectrometry-based detection method to demonstrate slow decarboxylation occurs within a 24 hour time period in solution, confirming the conversion of **Int1'** to **Int3'** mimicking the natural activity of the enzyme with cinnamic acid occurs (Supplementary Fig 4a). We then took advantage of the distinct spectral change associated with cycloadduct formation to determine if cycloaddition with natural substrates can also be monitored in solution. Indeed, rapid mixing of the enzyme with cinnamic or sorbic acid substrates revealed spectral changes in the UV-Vis spectrum of prFMN similar to those observed with the alkyne inhibitors (Supplementary Fig 3b,c). This suggest that, for these substrates, cycloadduct(s) accumulate under multiple turnover conditions.

The *An*Fdc1 active site constrains cycloadduct conformation

While both **Int1'** and **Int3'** structures confirm 1,3-dipolar cycloaddition can occur with the prFMN^{iminium} cofactor, several features indicate a significant degree of strain in these cycloadduct(s). The phenylpropiolic acid **Int1'** structure deviates from ideal bond parameters both in the position of the inhibitor phenyl group (Cβ out-of-phenyl plane angle is ~24° as opposed to ideal 0°), the deviation of the 3-pyrroline ring (C1'-Cα-Cβ bond angle of ~99°, as compared to ideal 108°), prFMN tetrahedral C4a bond angles (C2-C4a-Cβ bond angle of ~103° *versus* ideal 109.5°of sp^3 C4α) as well as the elongated C4a-Cβ bond length of 1.7 Å (Fig 4a). Following decarboxylation, the position of the **Int3'** 3-pyrroline ring shifts (Fig 3c) to alleviate some of the phenyl group strain (Cβ out-of-plane angle reduced to ~16°) as well as the deviation of the 3-pyrroline ring (C1'-Cα-Cβ bond angle of ~111°; Cβ-C4a bond length of 1.65 Å). The protein does not alter in conformation when comparing the **Inhib/Int1'** and **Int3'** structures, with the notable exception of Glu282, which reorients to occupy the substrate/inhibitor carboxylate binding pocket in **Int3'** (a motion similar to the CO_2 for Glu282 exchange proposed to occur during catalysis, Fig 1). In the latter, Glu282 forms an interaction with the 3-pyrroline substrate-derived Cα (distance ~3.2 Å to either E282 oxygen; Fig 3a). Glu282 mediated proton donation or abstraction would interconvert **Int3'** with the putative prFMN C1' – alkyne adduct **Int2'** (the complex analogous to **Int2**; Fig 1). However, an 'unstrained' linear C1'-alkyne adduct –with a C1'-Cα≡Cβ angle of 180°– is sterically incompatible with the *An*Fdc1 active site, suggesting a highly strained **Int2'** (similar to strained cyloalkyne species[15]) connects the **Int1'** and **Int3'** species, providing a likely explanation for the extremely slow rate of **Int1'** decarboxylation.

Mutagenesis alleviates cycloadduct strain and impacts catalysis

As observed for the **Int2** E282Q structures, the strain observed in the **Int1'** and **Int3'** structures appears to be a direct consequence of the inherent restrictions imposed by the rigid *An*Fdc1 active site. The position of the substrate aromatic group appears constrained to remain π-stacked with the prFMN isoalloxazine ring, by virtue of steric interactions with the Phe437 sidechain located adjacent to the conserved Leu439. This in turn imposes restrictions on the extent by which the prFMN isoalloxazine ring system can deform upon

formation of a C4a-Cβ bond with substrate, as the flavin uracil ring is sandwiched between Ala172 on the *si* face and the substrate aromatic group at the *re* face. We constructed the F437L and L439G variants and determined the crystal structures in complex with phenylpropiolic acid, as well as the activity with cinnamic acid. We found both mutations severely compromised enzyme activity as judged from steady state turnover. In the case of L439G, a substantial increase of K_M was observed, while the F437L variant was only affected in k_{cat} confirming a key role for Phe437 in catalysis (Supplementary Fig 5b,d). In the corresponding phenylpropiolic acid adduct crystal structures for both variants, **Int1'** decarboxylation *in crystallo* was not observed, even following co-crystallisation and prolonged incubation (up to several weeks) prior to X-ray exposure. This lack of decarboxylation activity with **Int1'** was confirmed in solution (Supplementary Fig 4b). In the case of the L439G **Int1'** crystal structure (to 1.12 Å resolution), a modest reorientation of the substrate carboxyl group along with a minor reduction of the Cβ out-of-plane angle is observed, associated with a corresponding reorientation of the F437 phenyl ring (Fig 3d). The void created by the L439G mutation is filled with a water molecule located within hydrogen bonding distance of the **Int1'** carboxylate, reducing the hydrophobicity of the carboxylate binding pocket. In addition, the L439G void was partially filled by the phenyl group of a second phenylpropiolic acid molecule, bound at the entrance of the active site. This observation offers a possible explanation for the drastic increase of the observed K_M for cinnamic acid in the L439G (as opposed to F437L) mutant, as similar binding of a second cinnamic acid molecule could be required for decarboxylation by L439G. The hydrophobic nature of the carboxylic acid binding pocket has been implicated in the mechanism of other decarboxylases[16,17]. In marked contrast, the F437L mutation does not affect the carboxylate binding or conformation, but subtly alters the position of the substrate phenyl moiety (structure obtained to 1.08 Å resolution; Fig 3e,f). This reorientation, while retaining a strained conformation of the Cβ out-of-plane angle of ~25°, is associated with elongation of the Cβ-C4a bond to 1.8 Å. It thus appears the Phe437 side chain counteracts the forces exerted on the prFMN 3-pyrroline ring through enzyme interactions with the **Int1'** carboxylate.

Smaller dipolarophile compounds form dead-end cycloadducts

Unfortunately, other mutations at the Phe437 position that could lead to further reduction of strain imposed by the 437 side-chain led to variants that did not bind the prFMN cofactor. We therefore co-crystallised the WT enzyme with 2-butynoic acid, avoiding the enzyme imposed adduct strain by interactions with the missing substrate phenyl moiety. In this case, an **Int1'^{butynoic}** structure was obtained to 1.02 Å resolution, revealing no decarboxylation had occurred (Fig 3g). Furthermore, the **Int1'^{butynoic}** is markedly different from the strained phenylpropiolic acid derived **Int1'** structure (Fig 3h). Little to no features associated with a strained **Int1'** configuration can be observed in the case of **Int1'^{butynoic}**, a consequence of repositioning of the prFMN^{iminium} C4a and associated uracil plane. This repositioning leads to a near ideal conformation of the **Int1'^{butynoic}** 3-pyrroline ring, with a reduced Cβ-C4a bond length of 1.56 Å and a C1'-Cα-Cβ bond angle of ~107°, but is incompatible with the presence of a substrate phenyl group held within the context of either the WT or F437L variant structures. As a consequence of the uracil plane repositioning, the prFMN O1 has moved out of the oxyanion binding-pocket formed by Q191 and two water molecules.

Decarboxylation of **Int1'**, and by similarity **Int1**, is likely assisted by the relatively hydrophobic nature of the carboxylate binding pocket, and ring opening of the strained cycloadduct to **Int2'/Int2**. It is however unclear what drives the cycloelimination step from **Int3** to product release, a process not observed for **Int3'**. Careful analysis of electron density associated with rapidly flash-cooled WT crystals incubated with cinnamic acid reveals this can be modeled as a mixture of 30% **Int3** and a 40% product complex (the remainder corresponding to the inactive hydroxylated prFMN species), suggesting cycloelimination is the rate limiting step under these conditions, as has previously been suggested[13] (to 1.24 Å resolution; Fig 2d). As observed with the **Int3'** structure, the **Int3** Cβ has an out-of-plane angle of ~13°, with additional strain observed for the Cα-Cβ-Cγ angle of ~122°, both associated with the tight hold the enzyme exerts on the substrate phenyl moiety and resulting in an C1' *endo* envelope conformation of the pyrrolidine ring (as opposed to the N *endo* conformation of the **Int3'** enforced by the Cα-Cβ double bond (Fig 4a). Hence, to determine how **Int3** strain might assist cycloelimination, we determined the structure of an **Int3^{crotonic}** species (to 1.39 Å resolution), obtained by co-crystallisation with crotonic acid (2-butenoic acid; Fig 2e). A comparison of **Int3^{crotonic}** with the cinnamic acid **Int3** (Fig 2f) reveals the **Int3^{crotonic}** pyrrolidine ring adopts a distinct envelope conformation with the N in *endo* position, that allows the prFMN^{iminium} C1' to adopt a more in-plane position, resembling the **Int3'** geometry. The **Int3^{crotonic}** conformation cannot be adopted by the cinnamic acid **Int3**, as severe clashes between the substrate phenyl ring and the active site occur. We suggest the lack of strain in the **Int3^{crotonic}** species is coupled to the fact no cycloelimination can be observed for this species, while a strained conformation such as that observed for cinnamic acid **Int3** is required for progression along the catalytic cycle.

Combining the various crystal structures of **Sub/Inhib**, **Int1'/Int2** and **Int3'** complexes with our solution data leads to a comprehensive overview of the *An*Fdc1 catalytic cycle (Fig 4). The rigid *An*Fdc1 active site brings the substrate into close proximity of the prFMN^{iminium} cofactor, aligning the Cα-Cβ double bond (or triple bond in case of alkyne inhibitors) with the C1'-N5-C4a azomethine ylide to poise the complex for cycloaddition. Formation of a pyrrolidine adduct between a similar putative encounter complex of cinnamic acid and free prFMN^{iminium} in solution would be accompanied by repositioning of both the Cα-Cβ substituents (*i.e.* carboxylate/benzyl group), as well as the prFMN uracil moiety. This is a direct consequence of the ring formation and the accompanying sp^2 to sp^3 change for substrate Cα/Cβ and prFMN C1'/C4a carbon atoms. However, within the confines of the enzyme active site, the extent to which reorientation can occur is limited. In fact, the enzyme active site appears evolved to have maximum complementarity with the substrate and product complexes, and hence constrains both the substrate carboxylate and phenyl moieties to adopt a position resembling the substrate complex throughout catalysis. In the case of the **Int1'^{butynoic}** and **Int3^{crotonic}** adducts, the lack of a phenyl moiety allows for a more relaxed conformation of the substrate/prFMN^{iminium} adduct within the confines of the active site. Crucially, neither **Int1'^{butynoic}** decarboxylation nor **Int3^{crotonic}** cycloelimination are observed suggesting that strain contributes to catalysis for both these steps.

Europe PMC Funders Author Manuscripts

Computational studies provide further insight into the *An*Fdc1 catalytic cycle

An active 'cluster' site model comprising ~ 230 atoms was built from the E282Q **Int2** X-ray crystal structure. The positions of peripheral atoms were fixed to maintain a crystal structure-like geometry, in addition to constraining the position of the F437 and L439 side chains in most calculations to allow their contribution to strain in the adducts to be investigated. Stable models of each species as identified in Fig 1 were found for cinnamic acid, phenylpropiolic acid and crotonic acid. In the case of cinnamic acid, cycloaddition (**Sub** → **Int1**) was found to occur as a 2-step reaction, via a ring-open covalent adduct (**Int1^{open}**), which possesses an unusual Cβ–C4a interaction (2.60 Å) in addition to a Cα–C1' bond (1.58 Å). The barrier to formation of the ring-closed **Int1** intermediate is small (Fig 5), so the reaction may effectively occur as one asynchronous step. In contrast, no stable **Int1^{open}**-type intermediates were observed for phenylpropiolic or crotonic acid cycloaddition, which also leads to significantly more stable **Int1** cycloadducts.

Cinnamic acid decarboxylation occurs from the ring-open **Int1^{open}** species and the **Int1^{open}** → **Int2^{CO2}** potential barrier is relatively low at ~ 16 kJ mol^{-1} (Fig 5). The barriers for phenylpropiolic and crotonic acid decarboxylation were not determined, but may be much higher than for cinnamic acid and/or occur via a different mechanism, as these reactions cannot proceed via an **Int1^{open}** intermediate and the decarboxylation of these is then significantly endothermic. In all cases, the **Int2^{CO2}**, which contain noncovalently bound CO_2, remain ring-open with broken (~3 Å) Cβ-C4a bonds. The crotonic acid derived **Int2^{CO2}** is most stable as it can adopt an unstrained ring-open conformation with near-ideal Cα–Cβ geometry. In contrast, both cinnamic acid and phenylpropiolic **Int2^{CO2}** intermediates adopt strained conformations with non-linear Cα–Cβ–Phenyl angles. Relaxation of the side chain constraints of Phe437 and Leu439, as a proxy of the F437L and L439G variants, relieves ~14 kJ mol^{-1} of strain from the cinnamic acid derived **Int2^{CO2}** adduct consistent with the role of these residues in constraining the geometry of the phenyl moiety of the adducts.

Once the CO_2 has vacated the active site, Glu282 mediated protonation of Cβ leads to the formation of a ring-closed **Int3** species for all compounds. The release of CO_2 and Cβ protonation were not studied in detail, as these reactions require substantial rearrangement of Glu282, which would require much larger models. Cycloelimination (**Int3** → **Prod**) to form non-covalently bound product complexes is exothermic and likely to be rate limiting in all three cases (Fig 5). Formation of styrene is the least exothermic (38 kJ mol^{-1}), while cycloelimination of phenylacetylene is highly unfavorable, being 81 kJ mol^{-1} uphill and likely proceeding via a barrier > 100 kJ mol^{-1} (not determined). Similarly, the barrier to propylene cycloelimination is estimated at ~100 kJ mol^{-1}. This is in agreement with our observation that turnover does not occur with either crotonic or phenylpropiolic acid, with the reaction stalling at the **Int3** stage. Crucially, in the case of cinnamic acid, the cycloelimination barrier was determined to be feasible, at 64 kJ mol^{-1} and 78.5 kJ mol^{-1} in the constrained and F437/L439-relaxed models respectively. The 14.4 kJ mol^{-1} difference is at least qualitatively consistent with the ~30 fold decrease in k_{cat} observed in the F439L variant (which retains some element of strain).

Discussion

In the case of the Fdc branch of the UbiD family, our data unambiguously establishes that the enzyme relies on covalent catalysis by the unusual prFMN cofactor through a reversible 1,3-dipolar cycloaddition process. The fact the active site is highly complementary in shape to the substrate/prFMN^{iminium} complex prior to cycloaddition has the serendipitous consequence it does not yield to allow pyrrolidine ring substituents to adopt the ideal conformation. This results in the formation of strained intermediates, ensuring rapid progression through the catalytic cycle. While substrate distortion/ground state destabilization has long been suggested to contribute to enzyme catalysis[18,19], it has only been conclusively demonstrated in a limited number of cases[20,21], and rarely includes atomic resolution insights[22–25]. Our study reveals in *An*Fdc1 distortion occurs specifically for covalent substrate-cofactor adducts only, and the strain is directly linked to progression along the reaction coordinate. Hence, by targeted destabilization of intermediate species only, *An*Fdc1 harnesses 1,3-dipolar cycloaddition as a readily reversible reaction. This aligns with the proposals from Albery and Knowles[26] for evolution of an efficient enzyme by control of the internal thermodynamics of the bound states. Interestingly, many members of the UbiD family act directly on aromatic substrates, and can act in the carboxylative direction as suggested for the anaerobic degradation of benzene[27,28]. (De)carboxylation of aromatic substrates presents a large inherent barrier to cycloaddition due to transient substrate dearomatisation, as well as scope for formation of a highly stable **Int2** adduct by re-aromatisation[29]. How these problems are overcome, particularly in view of whether the prFMN-dependent catalysis in these enzymes is similar to the Fdc branch, awaits a more detailed analysis of additional members of the UbiD family. Finally, our data suggests mechanochemical reversion of 1,3-dipolar cycloaddition reactions is feasible, providing further support to the possibility of developing mechanoresponsive materials through reversible click-chemistry[8–11]. Our data show Nature is able to harness and control 1,3-dipolar cycloaddition chemistry by combination of a unique cofactor with strict mechanochemical control.

Methods

See Supplementary Information for methods.

Supplementary Material

Refer to Web version on PubMed Central for supplementary material.

Acknowledgements

This work was supported by the grants BBSRC BB/K017802 and ERC pre-FAB 695013. The authors acknowledge the assistance given by the use of the Manchester Protein Structure Facility. We thank Diamond Light Source for access (proposal numbers MX12788 and MX17773) that contributed to the results presented here. D.L. is a Royal Society Wolfson Merit Award holder.

Data availability

The data generated and analysed in this study, including the computational modeling data associated with all figures, are available from the corresponding authors upon reasonable request. The diffraction data and corresponding atomic models have been deposited in the PDB under accession codes 6R3G, 6R3F, 6R3I, 6R2Z, 6R30, 6R3O, 6R2T, 6R2R, 6R3N, 6R3L, 6R3J, 6R2P, 6R34, 6R33 and 6R32.

References

1. Toney MD. Controlling reaction specificity in pyridoxal phosphate enzymes. Biochim Biophys Acta - Proteins Proteomics. 2011; 1814:1407–1418.
2. Kluger R, Tittmann K. Thiamin diphosphate catalysis: Enzymic and nonenzymic covalent intermediates. Chem Rev. 2008; 108:1797–1833. [PubMed: 18491870]
3. Piano V, Palfey BA, Mattevi A. Flavins as Covalent Catalysts: New Mechanisms Emerge. Trends Biochem Sci. 2017; 42:457–469. [PubMed: 28274732]
4. Marshall SA, Payne KAP, Leys D. The UbiX-UbiD system: The biosynthesis and use of prenylated flavin (prFMN). Arch Biochem Biophys. 2017; 632:209–221. [PubMed: 28754323]
5. Pellissier H. Asymmetric 1,3-dipolar cycloadditions. Tetrahedron. 2007; 63:3235–3285.
6. Jeon B-S, et al. Investigation of the mechanism of the SpnF-catalyzed [4+2]-cycloaddition reaction in the biosynthesis of spinosyn A. Proc Natl Acad Sci U S A. 2017; 114:10408–10413. [PubMed: 28874588]
7. Meldal M, Tornøe CW. Cu-Catalyzed Azide–Alkyne Cycloaddition. Chem Rev. 2008; 108:2952–3015. [PubMed: 18698735]
8. Jacobs MJ, Schneider G, Blank KG. Mechanical Reversibility of Strain-Promoted Azide-Alkyne Cycloaddition Reactions. Angew Chemie Int Ed. 2016; 55:2899–2902.
9. Khanal A, Long F, Cao B, Shahbazian-Yassar R, Fang S. Evidence of Splitting 1,2,3-Triazole into an Alkyne and Azide by Low Mechanical Force in the Presence of Other Covalent Bonds. Chem - A Eur J. 2016; 22:9760–9767.
10. Krupička M, Dopieralski P, Marx D. Unclicking the Click: Metal-Assisted Mechanochemical Cycloreversion of Triazoles Is Possible. Angew Chemie Int Ed. 2017; 56:7745–7749.
11. Stauch T, Dreuw A. Force-induced retro-click reaction of triazoles competes with adjacent single-bond rupture. Chem Sci. 2017; 8:5567–5575. [PubMed: 30155228]
12. Payne, KaP; , et al. New cofactor supports α,β-unsaturated acid decarboxylation via 1,3-dipolar cycloaddition. Nature. 2015; 522:497–501. [PubMed: 26083754]
13. Ferguson KL, Eschweiler JD, Ruotolo BT, Marsh ENG. Evidence for a 1,3-Dipolar Cyclo-addition Mechanism in the Decarboxylation of Phenylacrylic Acids Catalyzed by Ferulic Acid Decarboxylase. J Am Chem Soc. 2017; 139:10972–10975. [PubMed: 28753302]
14. Bailey SS, et al. The role of conserved residues in UbiD/Fdc decarboxylase in oxidative maturation, isomerisation and catalysis of prenylated flavin mononucleotide. J Biol Chem. 2018; 293:2272–2287. [PubMed: 29259125]
15. Borden WT. Pyramidalized Alkenes. Chem Rev. 1989; 89:1095–1109.
16. Okrasa K, et al. Structure and Mechanism of an Unusual Malonate Decarboxylase and Related Racemases. Chem - A Eur J. 2008; 14:6609–6613.
17. Jez JM, Ferrer JL, Bowman ME, Dixon RA, Noel JP. Dissection of malonyl-coenzyme A decarboxylation from polyketide formation in the reaction mechanism of a plant polyketide synthase. Biochemistry. 2000; 39:890–902. [PubMed: 10653632]
18. Blake CC, et al. Crystallographic studies of the activity of hen egg-white lysozyme. Proc R Soc London Ser B, Biol Sci. 1967; 167:378–88. [PubMed: 4382801]
19. Vocadlo DJ, Davies GJ, Laine R, Withers SG. Catalysis by hen egg-white lysozyme proceeds via a covalent intermediate. Nature. 2001; 412:835–838. [PubMed: 11518970]

20. Anderson VE. Quantifying energetic contributions to ground state destabilization. Arch Biochem Biophys. 2005; 433:27–33. [PubMed: 15581563]
21. Zhang Y, Schramm VL. Ground-State Destabilization in Orotate Phosphoribosyltransferases by Binding Isotope Effects. Biochemistry. 2011; 50:4813–4818. [PubMed: 21526795]
22. Lehwess-Litzmann A, et al. Twisted Schiff base intermediates and substrate locale revise transaldolase mechanism. Nat Chem Biol. 2011; 7:678–684. [PubMed: 21857661]
23. Milić D, et al. Crystallographic snapshots of tyrosine phenol-lyase show that substrate strain plays a role in C-C bond cleavage. J Am Chem Soc. 2011; 133:16468–16476. [PubMed: 21899319]
24. Vladimirova A, et al. Substrate Distortion and the Catalytic Reaction Mechanism of 5-Carboxyvanillate Decarboxylase. J Am Chem Soc. 2016; 138:826–836. [PubMed: 26714575]
25. Lüdtke S, et al. Sub-ångström-resolution crystallography reveals physical distortions that enhance reactivity of a covalent enzymatic intermediate. Nat Chem. 2013; 5:762–767. [PubMed: 23965678]
26. Albery WJ, Knowles JR. Efficiency and Evolution of Enzyme Catalysis. Angew Chemie Int Ed English. 1977; 16:285–293.
27. Abu Laban N, Selesi D, Rattei T, Tischler P, Meckenstock RU. Identification of enzymes involved in anaerobic benzene degradation by a strictly anaerobic iron-reducing enrichment culture. Environ Microbiol. 2010; 12:2783–2796. [PubMed: 20545743]
28. Luo F, et al. Metatranscriptome of an anaerobic benzene-degrading, nitrate-reducing enrichment culture reveals involvement of carboxylation in benzene ring activation. Appl Environ Microbiol. 2014; 80:4095–4107. [PubMed: 24795366]
29. Baunach M, Hertweck C. Natural 1,3-dipolar cycloadditions. Angew Chemie - Int Ed. 2015; 54:12550–12552.

Europe PMC Funders Author Manuscripts

Europe PMC Funders Author Manuscripts

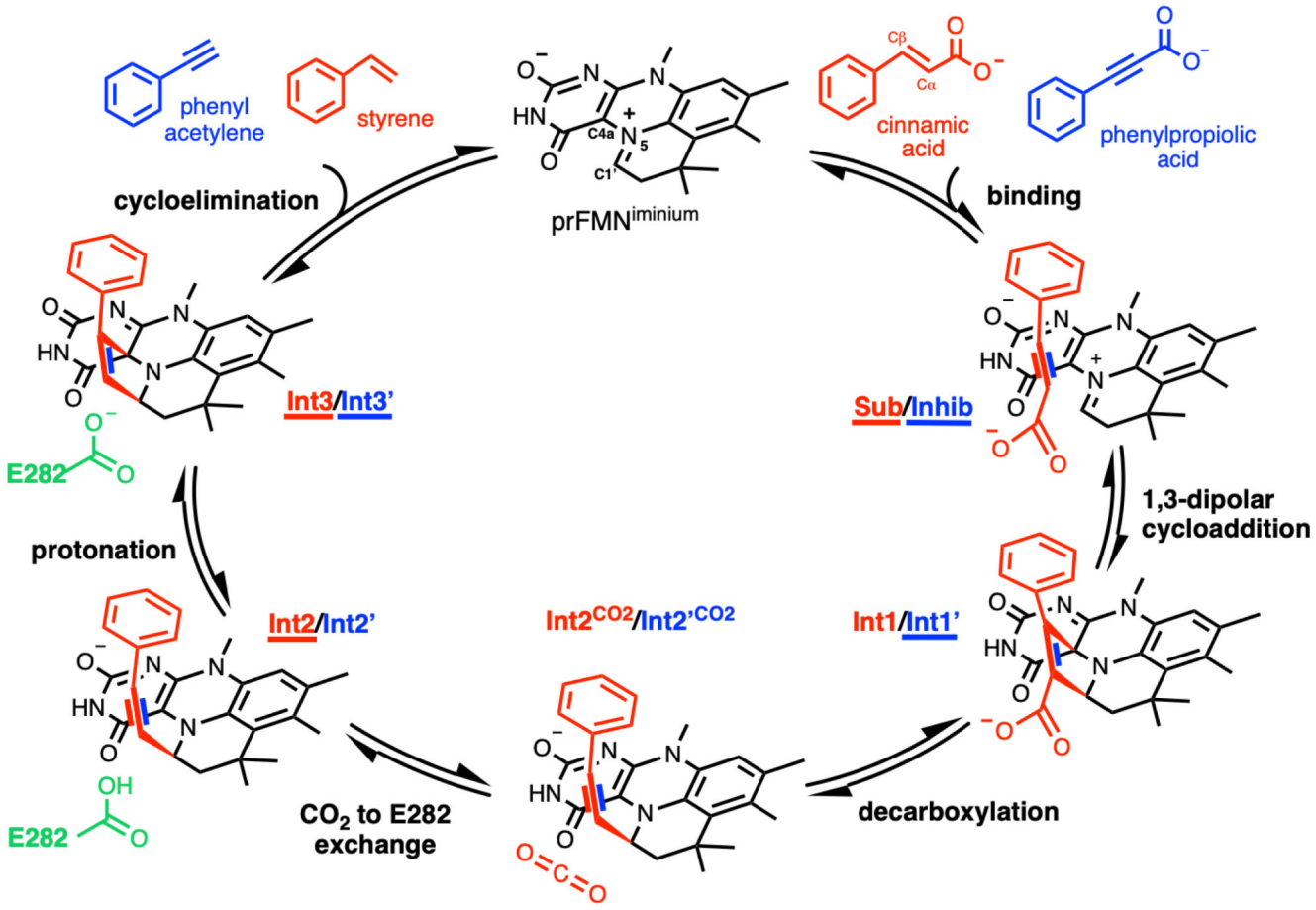

Fig 1. *A. niger* Fdc proposed enzyme mechanism.

The decarboxylation of cinnamic acid (in red) or the alkyne substrate analogue phenylpropiolic acid (in blue) by covalent catalysis using the prFMN^{iminium} cofactor (in black) is shown. Following the binding step, a 1,3-dipolar cycloaddition between the dipolarophile ligand and the azomethine ylide cofactor leads to the first cycloadduct species **Int1**. The additional unsaturated bond shown in blue highlights the reaction with the alkyne substrate analogue. Decarboxylation occurs concomitant with ring opening and formation of **Int2**. The bound CO_2 leaves the active site and is replaced by the E282 side chain (shown in green). Protonation via E282 leads to formation of a second cycloadduct species **Int3**. A cycloelimination process leads to formation of styrene and the entire reaction cycle is freely reversible. The labels for species for which crystal structures are determined here are underlined.

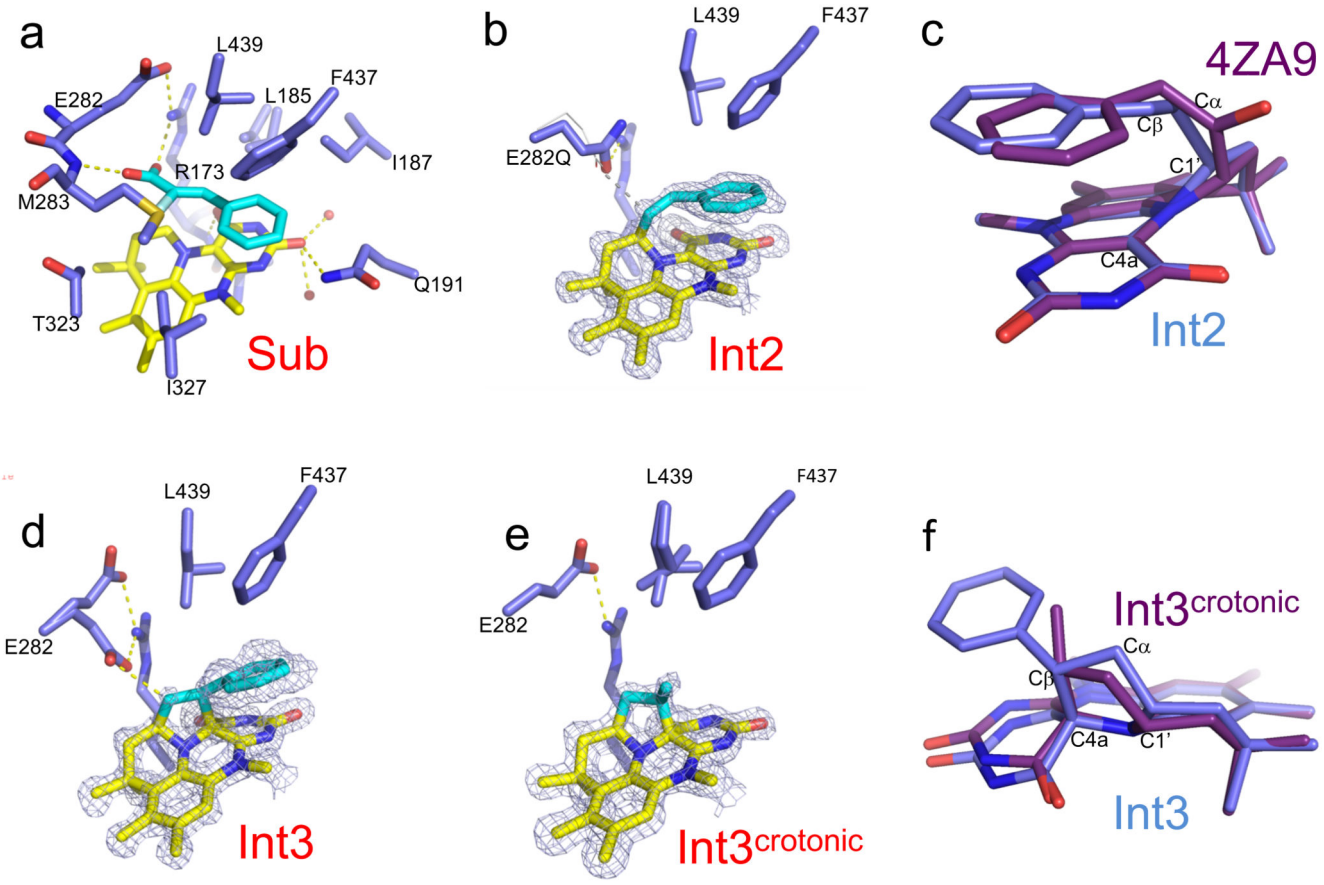

Fig. 2. Crystal structures of *A. niger* Fdc with propionic acid substrates.

a. Active site structure of Fdc in complex with alpha-fluorocinnamic acid. **b.** Omit electron density contoured at 4.5 sigma and corresponding model of the cinnamic acid **Int2** in the E282Q mutant. **c.** Overlay between the **Int2** E282Q covalent adduct formed and the adduct obtained with phenylpyruvate (PDB 4ZA9) **d**. Omit electron density contoured at 3 sigma and corresponding model of the cinnamic acid **Int3**. (populated at 30%) trapped by rapid flash-cooling of WT crystals following exposure to cinnamic acid (Supplementary Fig. 1 shows the product complex for comparison). **e.** Omit electron density contoured at 4 sigma corresponding to **Int3^{crotonic}**. **f.** Overlay between the **Int3** and **Int3^{crotonic}** acid covalent adducts formed.

Europe PMC Funders Author Manuscripts

Europe PMC Funders Author Manuscripts

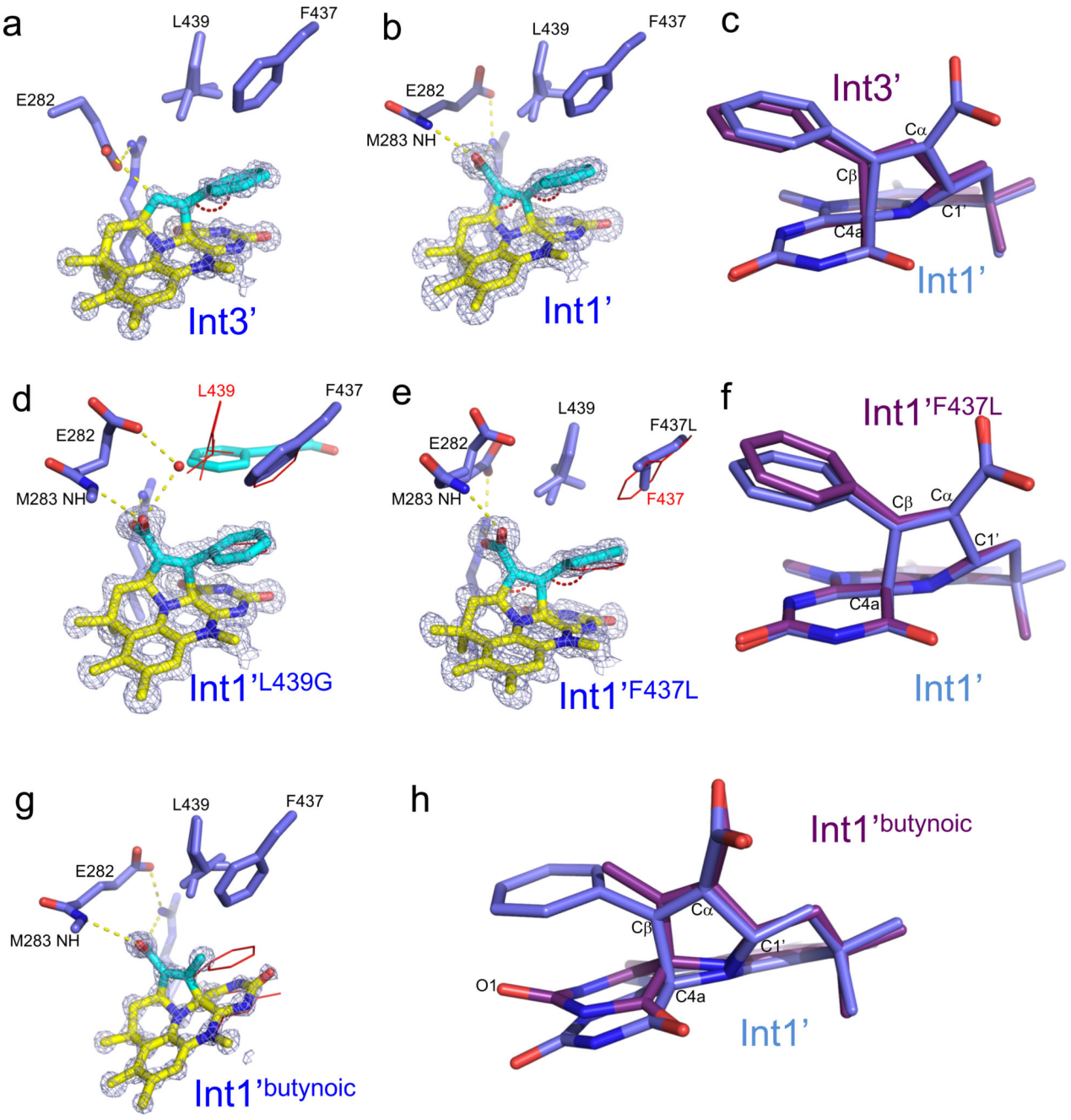

Fig 3. Crystal structures of *A. niger* Fdc with propiolic acid substrate analogues.

a. Omit electron density contoured at 5 sigma and corresponding model of the phenylpropiolic acid derived **Int3'** obtained through co-crystallisation (Calpha-C1' 1.52 Å and Cbeta-C4a 1.66 Å bond distances). **b.** Omit electron density contoured at 4 sigma and corresponding model of the phenylpropiolic acid derived **Int1'** obtained through soaking and rapid flash-cooling (Calpha-C1' 1.59 Å and Cbeta-C4a 1.70 Å bond distances). **c.** Overlay between the phenylpropiolic acid derived **Int1'** and **Int3'** covalent adducts formed. **d**. Omit electron density contoured at 4 sigma and corresponding model of the phenylpropiolic acid

derived **Int1'** for the L439G variant (Calpha-C1' 1.48 Å and Cbeta-C4a 1.86 Å bond distances). **e.** Omit electron density contoured at 4 sigma and corresponding model of the phenylpropiolic acid derived **Int1'** for the F437L variant (Calpha-C1' 1.51 Å and Cbeta-C4a 1.79 Å bond distances). **f.** Overlay between the **Int1'** adduct obtained in the WT and the F437L variant. **g**. Omit electron density contoured at 4 sigma and corresponding model of the 2-butynoic acid derived **Int1'^{butynoic}** (Calpha-C1' 1.52 Å and Cbeta-C4a 1.53 Å bond distances). **h.** Overlay between the **Int1'** and **Int1'^{butynoic}** adduct.

Europe PMC Funders Author Manuscripts

Europe PMC Funders Author Manuscripts

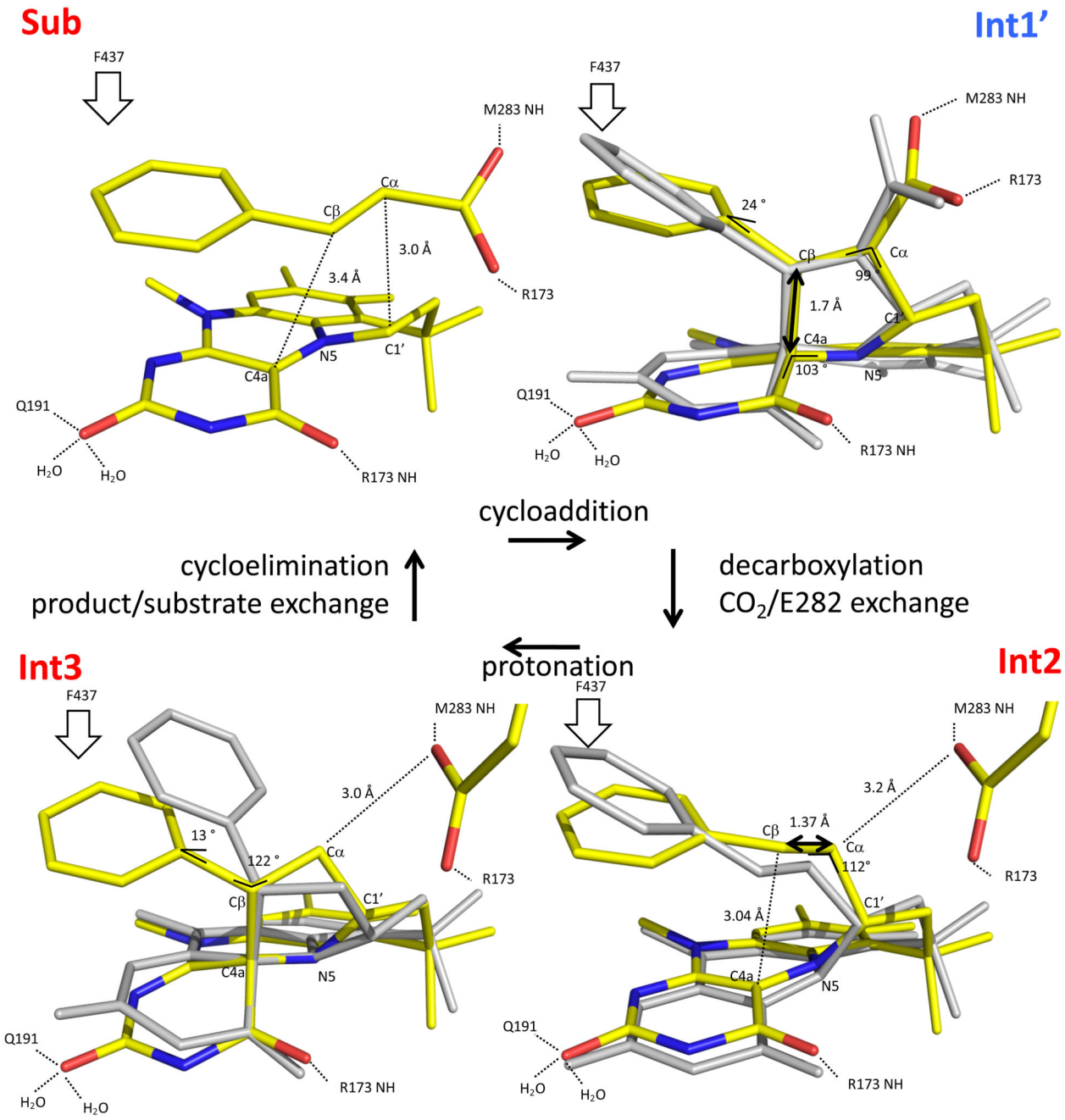

Fig. 4. The role of strain in the Fdc reaction.

Schematic overview of the structural insights gained into the Fdc reaction cycle. The prFMN^{iminium} cofactor and the substrate are shown for the various crystal structures of the **Sub/Int1'** (as a model for **Int1**)/**Int2** and **Int3** states. The active site restricts the position of the substrate phenyl ring throughout the reaction (as indicated by black arrow labelled F437), leading to formation of strained intermediates **Int1**/**Int2** and **Int3**. Substantial deviations from ideal bond lengths and angles are highlighted in black. For the **Int1'/Int2** and **Int3** species, DFT models of the corresponding prFMN adducts free in solution are

overlaid (coloured in grey). The differences observed for **Int1'** and **Int3** with respective DFT models of the corresponding unconstrained prFMN adducts resembles those observed when comparing **Int1'** and **Int3** with **Int1^{butynoic}** and **Int3^{crotonic}** (Figs 3h and 2f).

Europe PMC Funders Author Manuscripts

Europe PMC Funders Author Manuscripts

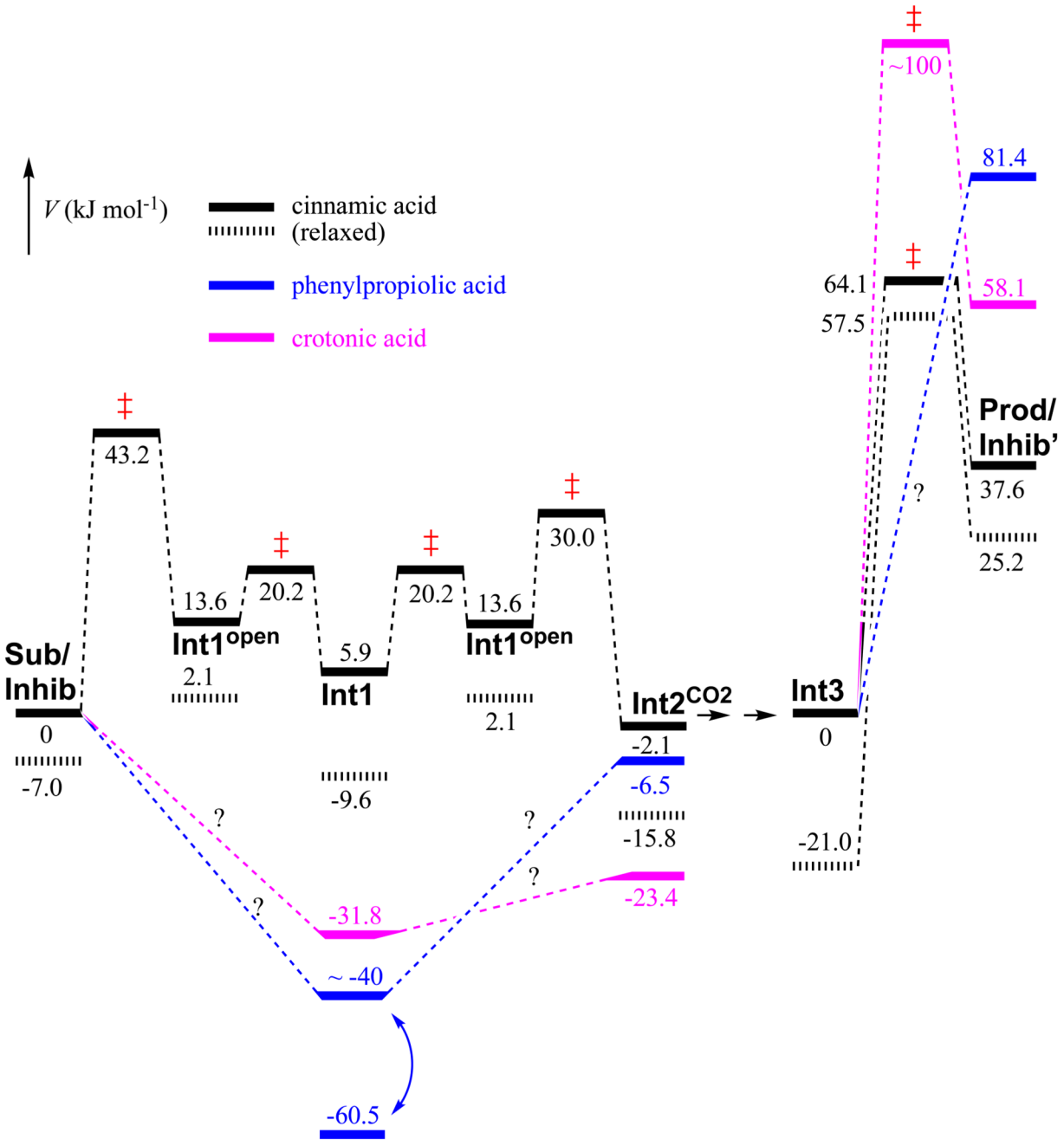

Fig. 5. Potential energy diagram of the Fdc reaction.

Potential energy diagram determined using DFT cluster models (Supplementary Figs 6,7), with potential energy normalised to the **Sub/Inhib** and **Int3** energies. The relaxed cinnamic acid energies were determined for models where restraints on the side chains of Phe437 and Leu439 were removed, which alleviates some of the strain on the Cβ–Ph bond (Supplementary Fig. 8). The two phenylpropiolic acid **Int1** species interconvert via rotation of the Cα–CO_2 bond and the conformation with the carboxyl group in the phenyl plane is the higher energy species and is not stable in the DFT model used here. The crotonic acid

Int3 → Prod transition state actually represents a minimum energy crossing point (Supplementary Figs. 9, 10).

Europe PMC Funders Author Manuscripts